

JGR Solid Earth

RESEARCH ARTICLE

10.1029/2018JB016859

Special Section:

Magnetism in the Geosciences
- Advances and Perspectives

Key Points:

- Sedimentary intervals rich in detrital magnetic mineral inclusions commonly record biased geomagnetic field intensity minima
- Redeposition experiments of inclusion-rich sediments indicate lower recording efficiency compared to inclusion-poor samples
- Variable recording efficiency of magnetic assemblages produces a bias that needs to be recognized in relative paleointensity records

Correspondence to:

L. Chang,
liao.chang@pku.edu.cn

Citation:

Hong, H., Chang, L., Hayashida, A., Roberts, A. P., Heslop, D., Paterson, G. A., et al. (2019). Paleomagnetic recording efficiency of sedimentary magnetic mineral inclusions: Implications for relative paleointensity determinations. *Journal of Geophysical Research: Solid Earth*, 124, 6267–6279. <https://doi.org/10.1029/2018JB016859>

Received 10 OCT 2018

Accepted 30 JUN 2019

Accepted article online 5 JUL 2019

Published online 22 JUL 2019

Paleomagnetic Recording Efficiency of Sedimentary Magnetic Mineral Inclusions: Implications for Relative Paleointensity Determinations

Hoabin Hong¹ , Liao Chang^{1,2} , Akira Hayashida³ , Andrew P. Roberts⁴ , David Heslop⁴ , Greig A. Paterson^{5,6} , Kazuto Kodama⁷ , and Lisa Tauxe⁸ 

¹Laboratory of Orogenic Belts and Crustal Evolution, School of Earth and Space Sciences, Peking University, Beijing, China, ²Laboratory for Marine Geology, Qingdao National Laboratory for Marine Science and Technology, Qingdao, China, ³Department of Environmental Systems Science, Doshisha University, Kyoto, Japan, ⁴Research School of Earth Sciences, Australian National University, Canberra, Australia, ⁵Department of Earth, Ocean and Ecological Sciences, University of Liverpool, Liverpool, UK, ⁶Key Laboratory of Earth and Planetary Physics, Institute of Geology and Geophysics, Chinese Academy of Sciences, Beijing, China, ⁷Research Center for Knowledge Science in Cultural Heritage, Doshisha University, Kyoto, Japan, ⁸Scripps Institution of Oceanography, University of California, San Diego, La Jolla, CA, USA

Abstract Sedimentary relative paleointensity (RPI) records are often carried by complex magnetic mineral mixtures, including detrital and biogenic magnetic minerals. Recent studies have demonstrated that magnetic inclusions within larger detrital silicate particles can make significant contributions to sedimentary paleomagnetic records. However, little is known about the role such inclusions play in sedimentary paleomagnetic signal recording. We analyzed paleomagnetic and mineral magnetic data for marine sediment core MD01-2421 from the North Pacific Ocean, offshore of central Japan, to assess how magnetic inclusions and other detrital magnetic minerals record sedimentary paleomagnetic signals. Stratigraphic intervals in which abundant magnetic inclusions dominate the magnetic signal are compared with other intervals to assess quantitatively their contribution to sedimentary RPI signals. The normalized remanence record from core MD01-2421 does not correlate clearly with global RPI stacks, which we attribute to a demonstrated lower paleomagnetic recording efficiency of magnetic inclusions compared to other detrital magnetic minerals. We also carried out the first laboratory redeposition experiments under controlled Earth-like magnetic fields for particles with magnetic inclusions using material from core MD01-2421. Our results confirm that such particles can be aligned by ambient magnetic fields but with a lower magnetic recording efficiency compared to other detrital magnetic minerals, which is consistent with normalized remanence data from core MD01-2421. Our demonstration of the role of sedimentary magnetic inclusions should have wide applicability for understanding sedimentary paleomagnetic recording.

1. Introduction

Understanding recording processes associated with detrital remanent magnetization (DRM) acquisition is important in sedimentary paleomagnetism because records of changing geomagnetic directions and relative paleointensity (RPI) have been used widely to understand geomagnetic field variations and deep-Earth geodynamo processes (e.g., Guyodo & Valet, 1999; Valet et al., 2005). Such records are also used widely to date sedimentary sequences (e.g., Roberts et al., 2013). As well as being controlled by the ambient field strength, RPI signals can be affected by various factors associated with the magnetic minerals in a sedimentary sequence, such as grain size distributions and magnetic properties, and a range of external factors, such as salinity, bioturbation, and postdepositional compaction during sediment deposition and burial (e.g., Katari & Tauxe, 2000; Zhao et al., 2016). Our understanding of DRM acquisition mechanisms has improved as a result of numerical simulations of individual particles and flocs (Heslop, 2007; Heslop et al., 2006; Heslop et al., 2014; Shcherbakov & Sycheva, 2008, 2010) and laboratory-controlled redeposition experiments (Mittra & Tauxe, 2009; Tauxe et al., 2006). These experimental studies include time/field dependence (Katari & Tauxe, 2000; Quidelleur et al., 1995), different materials and water contents (Carter-Stiglitz et al., 2006; Jackson et al., 1991; Levi & Banerjee, 1990; Lu et al., 1990; Paterson et al., 2013; Valet et al., 2017), and flocculation (Katari & Tauxe, 2000; Mittra & Tauxe, 2009; Spassov & Valet, 2012; Van Vreumingen, 1993a,

1993b). However, understanding of RPI signal recording remains poor due to the complex effects of the afore-mentioned factors (Roberts et al., 2013).

Previous studies have investigated the effects of sediment composition on DRM acquisition, including clay (Blow & Hamilton, 1978; King, 1955), inorganic magnetite (Jackson et al., 1991; Lu et al., 1990; Van Vreumingen, 1993a, 1993b), and biogenic magnetite (Paterson et al., 2013; Valet et al., 2017). These studies demonstrate that inorganic and biogenic magnetite can be important sedimentary paleomagnetic signal carriers. Recently, Chang, Bolton, et al. (2016), Chang, Roberts, et al. (2016) suggested that magnetic mineral inclusions hosted within detrital silicate particles occur widely in marine sediments and that they represent a potentially important DRM recorder. Compared to other detrital magnetic mineral forms, which are generally treated as isolated particles, magnetic inclusions consist of fine ferrimagnetic mineral grains embedded within a coarser nonmagnetic host mineral. Magnetic inclusions occur abundantly in igneous rocks and are well known to be paleomagnetically important in igneous rocks (e.g., Evans et al., 1968; Feinberg et al., 2005, 2006; Tarduno et al., 2006; Usui et al., 2015). Magnetic inclusions are predominantly distributed over the fine-grained stable single-domain or vortex state size range (e.g., Harrison et al., 2002; Tarduno & Cottrell, 2005; Chang, Bolton, et al., 2016; Chang, Roberts, et al., 2016). Also, inclusions are enclosed and protected against surrounding environmental changes by their aluminosilicate hosts (e.g., plagioclase and pyroxene, which are abundant in igneous and metamorphic rocks). These characteristics mean that magnetic inclusions can potentially preserve stable remanent magnetizations over billions of years (Muxworthy et al., 2013; Renne et al., 2002; Selkin et al., 2000; Tarduno et al., 2006, 2010). Silicates can protect embedded magnetic inclusions from chemical alteration induced, for example, by hydrothermal fluids or oxidation in igneous rocks (Tarduno et al., 2006) or during reductive diagenesis in sediments (Chang, Bolton, et al., 2016). Magnetic inclusions within silicates in sediments could, therefore, be a potential recorder of sedimentary paleomagnetic signals, even for sediments that have been subjected to extensive chemical or mechanical alterations (e.g., postdepositional compaction and bioturbation).

Few studies have contributed to understanding how magnetic inclusions contribute to sedimentary paleomagnetic signals (e.g., Chang, Bolton, et al., 2016; Chen et al., 2017). In this study, we explore signals carried by magnetic inclusions through paleomagnetic analysis of marine sediment core MD01-2421 from offshore of Japan. This sediment core contains abundant magnetic inclusions, and the magnetic properties of some intervals are dominated by inclusions (Chang, Bolton, et al., 2016). We divide the sediment core into intervals with abundant magnetic inclusions and those with mixed detrital magnetic mineral assemblages (which we refer to as inclusion-rich and inclusion-poor intervals, respectively), based on their distinctive magnetic and geochemical properties. Such separation enables assessment of paleomagnetic recording behavior associated with sedimentary magnetic mineral inclusions. In addition, we present results of preliminary laboratory redeposition experiments using particles with magnetic inclusions from different intervals of the studied sediment core. Together, these results are used to assess DRM recording associated with magnetic inclusions.

2. Marine Sediment Core MD01-2421

The marine sediment core studied here, MD01-2421, is from the North Pacific Ocean, ~100 km offshore of central Japan (36°01.40'N, 141°46.80'E; 2,224-m water depth; 45.82 m long; Oba et al., 2006; Chang, Bolton, et al., 2016; Figure 1). The core was recovered from a location where the warm and saline subtropical Kuroshio Current and the cold and less saline subarctic Oyashio Current meet. The core was collected during the International Marine Global Change Study cruise VII-Western Pacific Margin Leg 2 of R/V *Marion Dufresne* in 2001 (Oba et al., 2006). The recovered sediments are homogenous olive-gray silty clays with calcareous and siliceous microfossils and high total organic carbon contents (0.5–2.1 wt %; Ueshima et al., 2006). The sediments were deposited continuously with a basal age of 144 ka and an average sedimentation rate of 30 cm/kyr in a hemipelagic environment (Oba et al., 2006). A detailed age model for the core is based on oxygen isotope stratigraphy from benthic foraminifera (Oba et al., 2006). The magnetic domain state of samples from core MD01-2421 spans a spectrum from stable single-domain to vortex state with high coercivity (i.e., $B_c > 30$ mT) to multidomain (MD) grains with low coercivity (i.e., $B_c < 20$ mT; Chang, Bolton, et al., 2016). Detailed magnetic measurements, including hysteresis properties, first-order reversal curve (FORC) diagrams, isothermal remanent magnetization (IRM), and thermomagnetic curves indicate consistently that

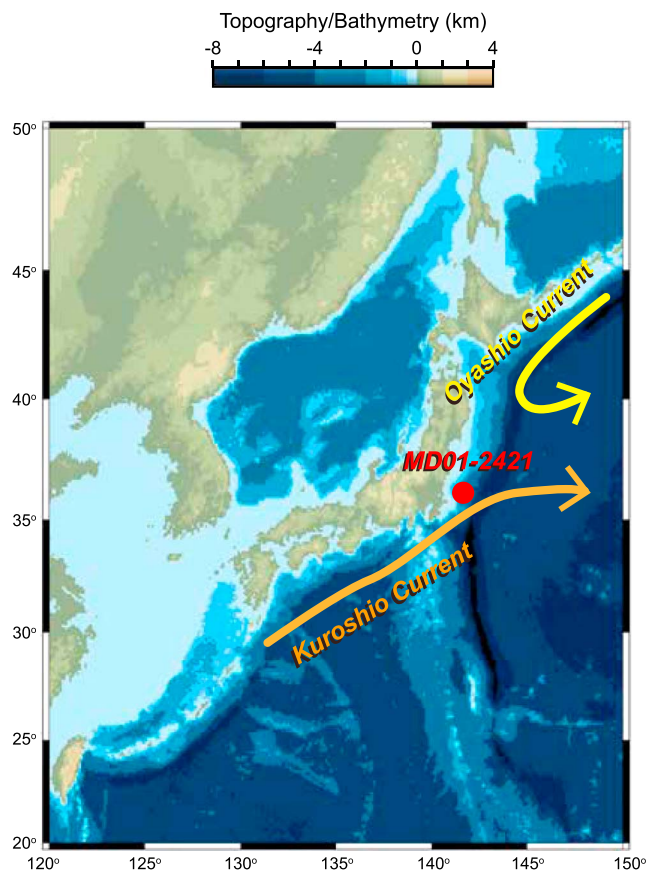


Figure 1. Location map of the studied marine sediment core MD01-2421 (red solid circle) in the North Pacific Ocean. The environment near the core location is affected by the cold Oyashio current (yellow arrow) and the warm Kuroshio current (orange arrow).

the constituent magnetic minerals are dominantly magnetite and titanomagnetite (Chang, Bolton, et al., 2016). Scanning electron microscope (SEM) and transmission electron microscope observations on magnetic extracts from the sediments reveal the presence of fine magnetic particles, including the widespread occurrence of magnetite/titanomagnetite nanoparticles hosted within silicates (Chang, Bolton, et al., 2016), in addition to coarse-grained and unprotected detrital magnetite/titanomagnetite grains.

3. Methods

3.1. Paleomagnetic and Rock Magnetic Measurements of u-Channels

Paleomagnetic data were obtained from the entire core from u-channel samples, which typically have 1.5-m length and 2×2 -cm square cross section. The natural remanent magnetization (NRM) of u-channels was measured at 1-cm intervals using a 2-G Enterprises 755R long-core cryogenic magnetometer with stepwise alternating field (AF) demagnetization carried out at 5-mT intervals from 0 to 20 mT at Doshisha University, Japan. Some u-channels were AF demagnetized up to 30 mT. Data from the top and bottom 5 cm of each u-channel were discarded to avoid edge effects. After AF demagnetization, an anhysteretic remanent magnetization (ARM) was imparted using a 100- μ T direct current (DC) bias field superimposed on a decaying 80-mT peak AF. ARM was measured first at Doshisha University and was then remeasured at Kochi Core Centre (KCC), Kochi University, Japan, with a 2-G Enterprises 755R long-core cryogenic magnetometer after a few years. Nearly identical results were found between the two measurement systems. ARM data from KCC were used in this paper. The translation speed used to impart an ARM to the u-channels at KCC was 10 cm/s. After ARM measurements, an IRM was imparted at 1 T using a pulse magnetizer, which was then measured with a 2-G Enterprises 755R long-core cryogenic magnetometer at KCC.

3.2. Magnetic Measurements on Discrete Samples and SEM Observations

In order to validate demagnetization results from u-channel samples, discrete samples were taken with paleomagnetic cubes for every section from the studied core (e.g., ~ 1.5 -m sampling interval). AF demagnetization was carried out in 12 steps for these samples (0, 2.5, 5, 10, 15, 20, 25, 30, 35, 40, 45, 50, 55, and 60 mT), and magnetizations were measured using a fluxgate spinner magnetometer (Natsuhara-Giken SMD-88) at Doshisha University. To understand paleomagnetic recording of magnetic inclusions, we carried out redeposition experiments in a controlled laboratory environment. Experimental DRM results for two samples from inclusion-rich (MD01-2421-10-100, 14.47 m, 42.91 ka) and inclusion-poor (MD01-2421-16-100, 23.3 m, 71.43 ka) intervals are compared: one sample contains mainly particles with magnetic inclusions (where other unprotected magnetic grains were dissolved diagenetically; red star in Figure 2), while the other sample contains a mixture of large, unprotected detrital grains and minor magnetic mineral inclusions within silicates (blue star in Figure 2). The two samples were characterized magnetically and with SEM observations. Hysteresis and FORC measurements were made with a Princeton Measurements Corporation vibrating sample magnetometer (model 3900) at the Paleomagnetism and Geochronology Laboratory, Institute of Geology and Geophysics, Chinese Academy of Sciences, Beijing. Hysteresis loops were measured between -1 and $+1$ T or between -500 and $+500$ mT with a field step of 5 mT and an averaging time of 250–300 ms. FORC diagrams (Pike et al., 1999; Roberts et al., 2000) were obtained with a 1 T maximum applied field, 2.7-mT field increments and 350-ms averaging time. FORC diagrams were produced with the FORCinel 3.0 software of Harrison and Feinberg (2008). Electron microscope observations were made using a FEI Quanta 650 field emission gun SEM at the School of Earth and Space Sciences, Peking University, China.

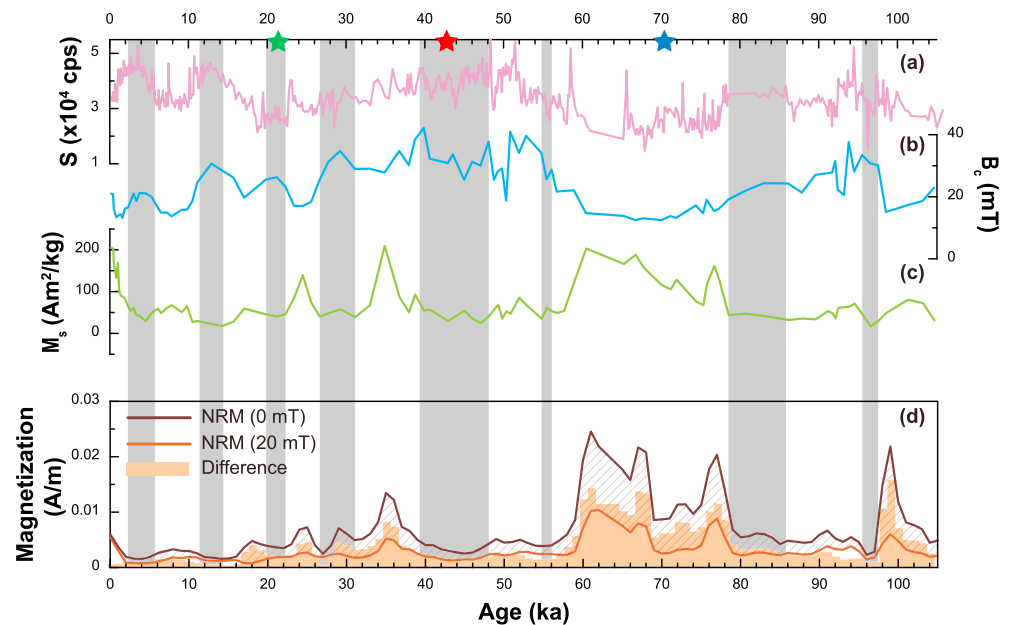


Figure 2. Down-core geochemical, magnetic, and paleomagnetic variations for core MD01-2421: (a) elemental S abundance, (b) coercivity (B_c), (c) saturation magnetization (M_s), and (d) paleomagnetic remanence after 0 (dark brown line) and 20 mT (brown line) and the difference between these steps (bright orange bar). Geochemical and magnetic data are from Chang, Bolton, et al. (2016). Gray bars mark magnetic inclusion-rich intervals with harder magnetic minerals, as indicated by high coercivity and high S abundance and weaker magnetization (e.g., lower M_s). Red and blue stars indicate stratigraphic positions of “inclusion-rich” and “inclusion-poor” samples used for laboratory redeposition experiments, respectively. Green (sample MD01-2421-7-110, 10.06 m, 21.21 ka; Chang, Bolton, et al., 2016) and red (MD01-2421-10-100, 14.47 m, 42.91 ka; section 3.2) stars indicate the stratigraphic positions of samples from which silicate grains have been observed from electron microscopic observations to contain magnetic mineral inclusions. NRM = natural remanent magnetization.

3.3. DRM Redeposition Experiments

Six air-dried sister specimens with similar mass were used for DRM experiments. For laboratory-controlled redeposition experiments, we used two orthogonal sets of Helmholtz coils. First, we mixed ~ 0.05 g of sediment with pure water and filled standard $2 \times 2 \times 2$ -cm paleomagnetic plastic cubes with the slurry. After shaking to randomize particle orientation, the cubes were put inside the Helmholtz coils. The sediment settled in a $60\text{-}\mu\text{T}$ field over 6 days. To prevent dust contamination, samples were covered during settling and drying. After drying completely, the redeposited sediment formed a thin layer at the base of each cube. Remanent magnetization measurements were made with a 2-G Enterprises DC superconducting quantum interference device rock magnetometer (model 755; noise level 3×10^{-12} A/m²) housed in a magnetically shielded room at Peking University. Magnetic susceptibility was measured with an AGICO MFK1-FA Kappabridge system. An ARM was imparted with a 100-mT peak AF and a $50\text{-}\mu\text{T}$ DC bias field. An IRM was imparted with an ASC IM-10-30 pulse magnetizer. Remanence was measured with the superconducting quantum interference device magnetometer. All DRM experiments and subsequent paleomagnetic measurements, except for ARM measurements, were carried out at Peking University. ARM measurements were made at the Paleomagnetism and Geochronology Laboratory, Institute of Geology and Geophysics, Chinese Academy of Sciences, Beijing.

4. Results

4.1. Paleomagnetic Behavior of Magnetic Mineral Inclusions in Core MD01-2421

4.1.1. Sedimentary Intervals Dominated by Magnetic Mineral Inclusions

Magnetic and geochemical property variations for core MD01-2421 (Figures 2a–2c), including coercivity (B_c), saturation magnetization (M_s), and elemental S abundance (Chang, Bolton, et al., 2016), have large down-core variations. Down-core trends of X-ray fluorescence S abundance and B_c are similar, but both

correlate inversely with M_s (Figure 2). These correlations indicate a strong relationship between the magnetic mineral assemblage and geochemical processes through reductive diagenesis (Chang, Bolton, et al., 2016). Magnetic minerals (both concentration and mineralogy) are influenced by variations in sulfidic diagenesis intensity through time (indicated by S variations), which control down-core B_c and M_s fluctuations. Unprotected magnetic particles, including detrital and biogenic magnetite, were dissolved, but fine-grained Fe-Ti oxide inclusions were preserved because they were protected by host silicate grains even under strongly sulfidic conditions (indicated by high sedimentary S contents) because silicates are largely unreactive to sulfide (Canfield et al., 1992; Poulton et al., 2004; Roberts, 2015; Chang, Roberts, et al., 2016). The dominant contribution of inclusions to the magnetic signal within strongly diagenetically altered sediment intervals is confirmed by transmission electron microscope observations and magnetic property variations (Chang, Bolton, et al., 2016; Chang, Roberts, et al., 2016). Based on these relationships, we isolated sediment intervals with abundant magnetic inclusions (gray bar in Figure 2). Criteria for defining these gray shaded intervals (Figure 2) are based on absolute values of B_c , M_s , and S and also on down-core data trends (i.e., increasing or decreasing), where “inclusion-rich” intervals (marked by gray shading) have relatively high B_c , low M_s , and high S values. These intervals are distinct from other intervals in which more diverse detrital magnetic mineral mixtures are present, including inclusions. The presence of silicate grains that contain magnetic mineral inclusions in core MD01-2421 has been validated by further SEM imaging (section 4.2) of magnetic mineral extracts and hand-picking of silicate single crystals in addition to the observations presented by Chang, Bolton, et al. (2016). It is not feasible to quantify the relative abundance of magnetic mineral inclusions throughout the core using direct electron microscopic observations; our distinction is based on down-core magnetic and geochemical profiles as proxies that can only provide an estimate of relatively inclusion-rich layers. Nevertheless, this approach enables a first-order separation of magnetic mineral inclusion-rich intervals from inclusion-poor intervals, so that their paleomagnetic recording behavior can be compared.

AF demagnetization results of discrete (Figures 3a and 3c) and u-channel samples (Figures 3b and 3d) for core MD01-2421 indicate that a viscous remanent magnetization component can be eliminated below 10 mT for both inclusion-rich (Figures 3a and 3b) and inclusion-poor samples (Figures 3c and 3d). This indicates that remanence after AF demagnetization at 10 mT is primary and should reflect different DRM behaviors between magnetic inclusion-rich and inclusion-poor samples. The difference in remanence is calculated from the NRM at 0 mT subtracted from the NRM after AF demagnetization at 20 mT. The difference in remanence between inclusion-rich and inclusion-poor samples is smaller after AF demagnetization at 20 mT (Figure 2d). The average differences between inclusion-rich and inclusion-poor samples are 1.9 and 5.0 A/m with standard deviations of 1.1 and 3.9 A/m, respectively. We plotted paleomagnetic data after AF demagnetization at 10 and 20 mT. Magnetic inclusions often occur within the tens of nanometer size range and have stable remanent magnetizations and high coercivities (e.g., Harrison et al., 2002; Feinberg et al., 2005; Tarduno & Cottrell, 2005; Chang, Roberts, et al., 2016). Intervals with significant magnetic inclusion contents (gray bars in Figures 2d), therefore, have relatively small differences between NRM and remanence after AF demagnetization at 20 mT compared to inclusion-poor intervals (Figure 2d), which is consistent with their more stable remanent magnetization. This confirms that our approach for isolating magnetic inclusion-rich intervals is appropriate.

4.1.2. Paleomagnetic Record of MD01-2421 Compared to Global RPI Stacks

Global paleointensity stacks, including the Sint-800 (Guyodo & Valet, 1999), PISO-1500 (Channell et al., 2009), and PADM2M stacks (Ziegler et al., 2011), are compared with the normalized remanence record of core MD01-2401 in Figures 4b–4d. Global stacks outline the general global trend of relative paleomagnetic intensity variations. Good correlation between the paleomagnetic record for core MD01-2421 and these global stacks is not expected because of large down-core changes in magnetic mineralogy, concentration, and grain size primarily due to magnetic mineral diagenesis (Chang, Bolton, et al., 2016). The purpose of our comparison is to identify potential paleomagnetic recording biases due to the complex magnetic mineralogy, including those due to magnetic inclusions. Normalized remanence records were obtained by normalizing NRM (after AF demagnetization at 10 and 20 mT) by susceptibility (k), ARM, and IRM (Figure 4). To minimize effects due to changing sedimentation rates between global stacks and the studied core, data for core MD01-2421 were computed using a 100-year moving average (Figures 4b–4d, darker colors). Normalized remanence records for core MD01-2421 are similar for three normalizers (Figures 4b–4d).

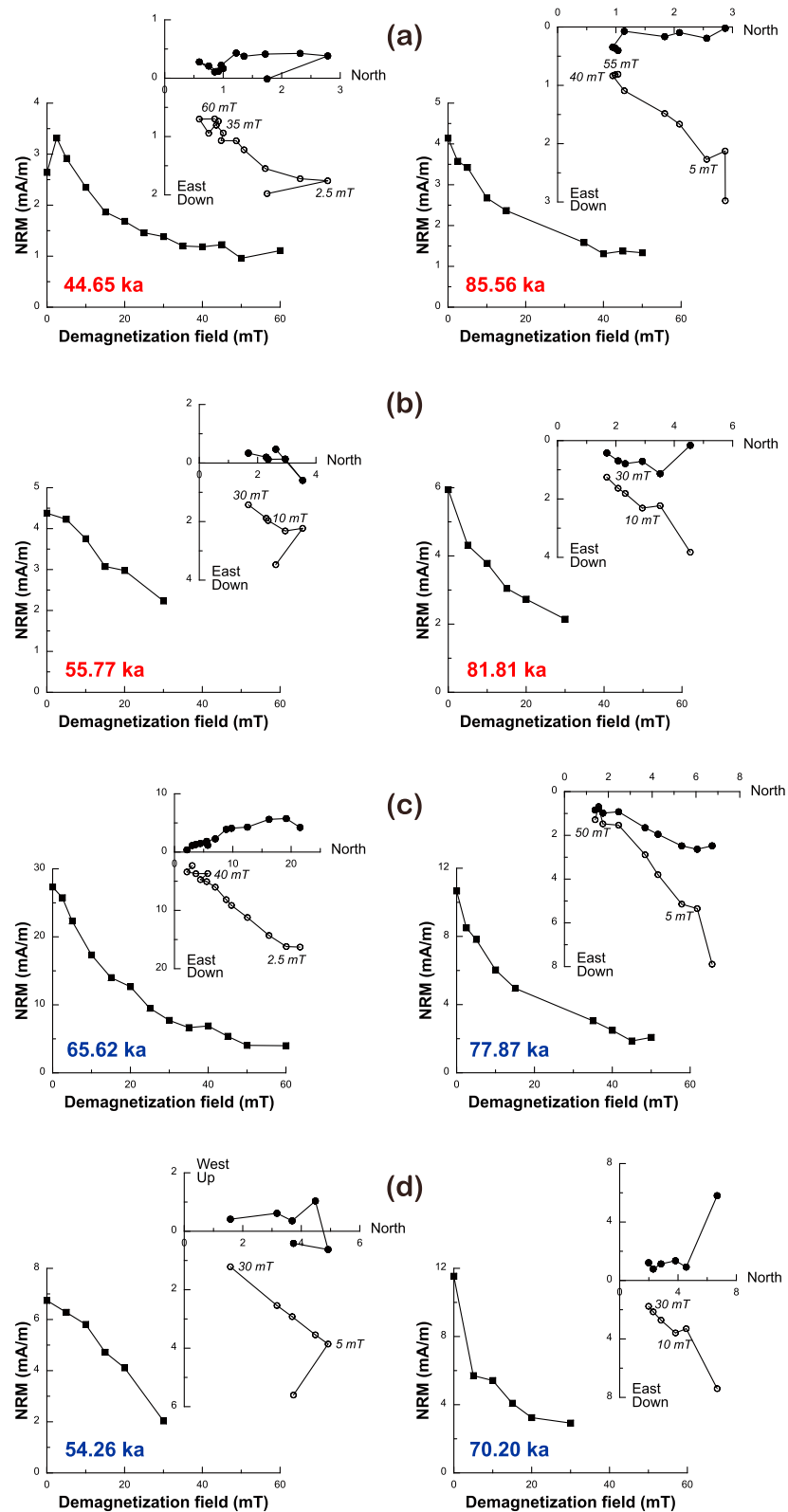


Figure 3. Representative alternating field-demagnetization results for discrete and u-channel samples for core MD01-2421. Solid and open circles represent projections onto the horizontal and vertical planes, respectively. (a, b) Inclusion-rich, (c, d) inclusion-poor intervals, (a, c) discrete samples, and (b, d) u-channel results. NRM = natural remanent magnetization.

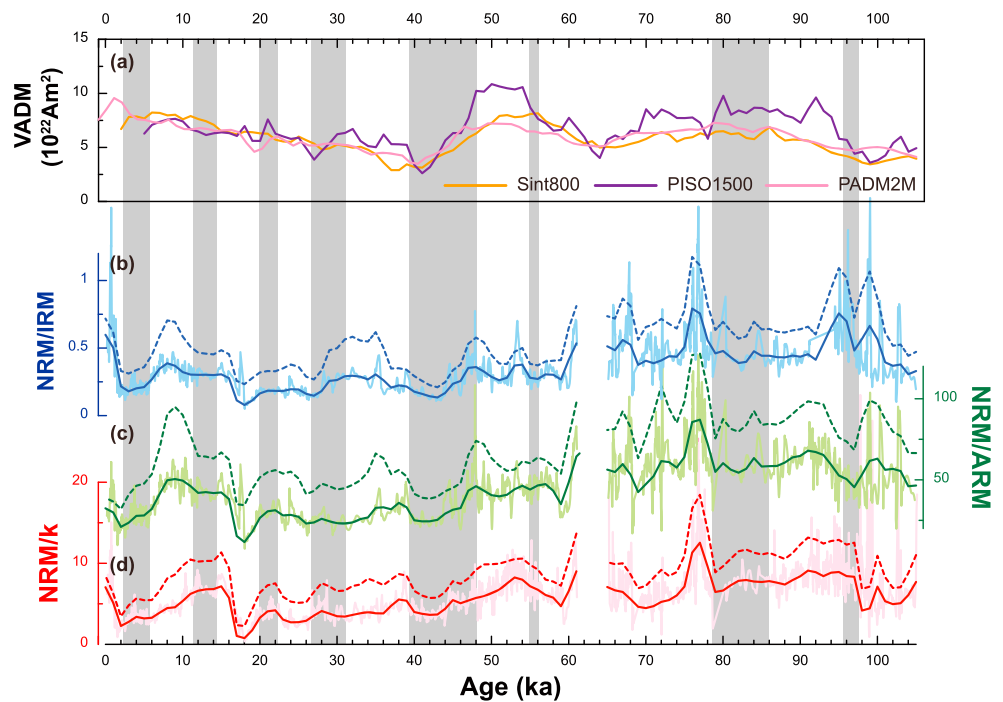


Figure 4. Comparison of (a) the Sint-800 (orange), PISO-1500 (purple), and PADM2M (pink) relative paleointensity stacks to the normalized remanence record of core MD01-2421 for (b) $\text{NRM}_{20}/\text{IRM}$ (blue), (c) $\text{NRM}_{20}/\text{ARM}$ (green), and (d) $\text{NRM}_{20}/\text{susceptibility}$ (red). Solid (dotted) lines are alternating field-demagnetization in 20 mT (10 mT), and the light color is the original data before calculating a 100-year moving average. Gray bars are the same as in Figure 2. VADM = virtual axial dipole moment; NRM = natural remanent magnetization; IRM = isothermal remanent magnetization; ARM = anhysteretic remanent magnetization.

There is poor correlation between the global RPI stacks and normalized remanence records for core MD01-2421 (Figure 4). Importantly, the normalized remanences generally have minimum values within magnetic inclusion-rich intervals (Figure 4). The weaker signals indicate that magnetic inclusions potentially induce a recording bias, although we cannot make definite conclusions from these data because of possible effects due to regional geomagnetic field differences with respect to the global field. We plot NRM (after AF demagnetization at 20 mT) versus ARM, IRM, and k separately for inclusion-rich and inclusion-poor intervals (Figures 5a–5c). Distinctly different slopes for linear fits are observed for the respective intervals, where the normalized NRM for inclusion-rich intervals has a lower slope compared to inclusion-poor intervals (Figures 5a–5c). These data support a lower recording efficiency of magnetic inclusions compared to other detrital magnetic minerals. An ARM versus k plot (Banerjee et al., 1981) indicates a dominance of finer particles for inclusion-rich intervals compared to inclusion-poor intervals (Figure 5d), but these finer particles have relatively low remanence recording efficiency. This is likely caused by the lower responsiveness of the relatively heavy nonmagnetic silicate host particles to alignment by geomagnetic torques.

4.2. Magnetic Properties and Laboratory Redeposition Experiments

Magnetic results and SEM observations for the two samples from inclusion-rich and inclusion-poor intervals used for redeposition experiments are shown in Figures 6 and 7, respectively. Magnetic properties are distinct for the two samples. Hysteresis loops have B_c values of 31 and 14 mT and a ratio of saturation remanence to saturation magnetization (M_{rs}/M_s) of 0.38 and 0.18 for samples from the inclusion-rich and inclusion-poor intervals, respectively (Figures 6a and 6b). Averages of B_c values for inclusion-rich and inclusion-poor intervals are 27.0 and 21.1 mT with standard deviations of 6.0 and 7.5 mT, respectively. The average M_{rs}/M_s ratio is 0.28 and 0.22 with standard deviations of 0.04 and 0.06 for inclusion-rich and inclusion-poor intervals, respectively. A FORC diagram for the sample from the inclusion-poor interval has vortex state/MD characteristics and low coercivities, while the magnetic inclusion-rich sample has a single domain/vortex state FORC distribution with higher coercivities (Figures 6c and 6d; Roberts et al., 2017).

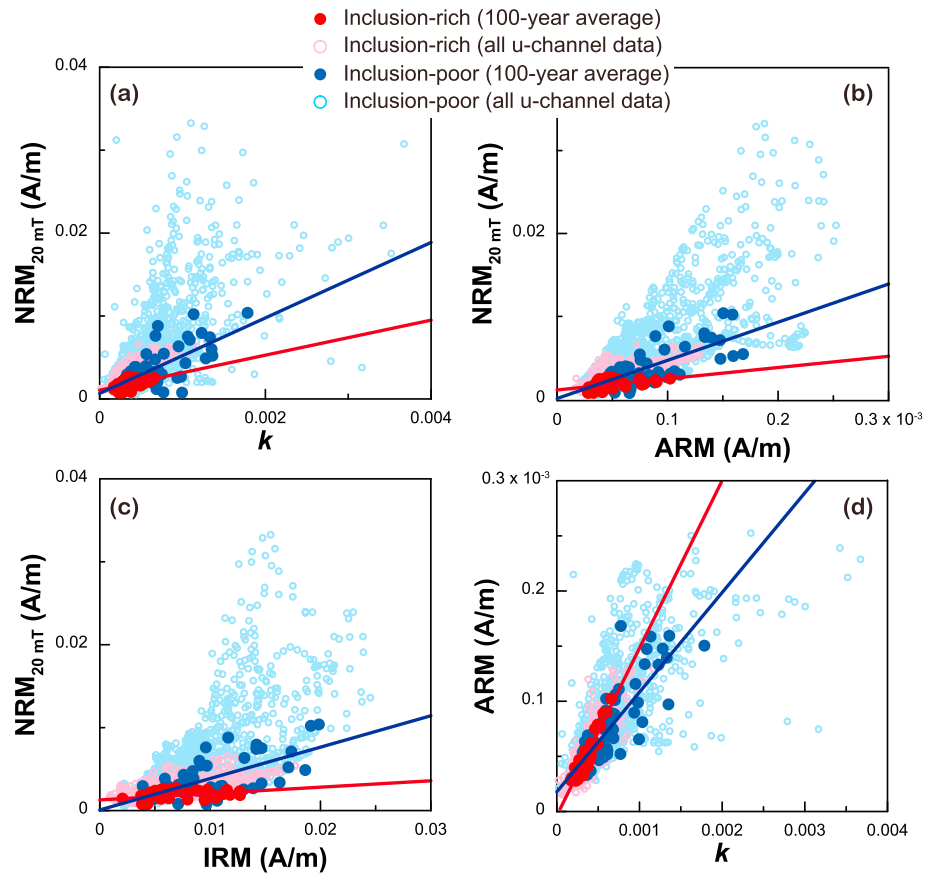


Figure 5. Comparison of paleomagnetic recording efficiency for “inclusion-rich” and “inclusion-poor” sediment intervals from core MD01-2421. NRM_{20mT} versus (a) susceptibility, (b) ARM, and (c) IRM and (d) ARM versus susceptibility (Banerjee et al., 1981). Lines are means for inclusion-rich (red) and inclusion-poor (blue) samples. All data are from u-channel samples. Darker (lighter) colors represent 100-year moving average (original) data. NRM = natural remanent magnetization; IRM = isothermal remanent magnetization; ARM = anhysteretic remanent magnetization.

These results are consistent with those reported for intervals from the same core by Chang, Bolton, et al. (2016). SEM observations of an inclusion-rich sample (MD01-2421-10-100, 14.47 m, 42.91 ka) indicate the presence of abundant silicate grains with magnetic nanoparticle inclusions (Figure 7).

We performed DRM experiments with wet or fully dried samples and observed nearly identical DRM results. Dried samples were, therefore, used for the following DRM experiments. Laboratory redeposition results for the inclusion-rich and inclusion-poor samples (red and blue, respectively) are shown in Figure 8. Declination of DRM is generally recorded as the set declination, with some scatter at 45° (Figure 8a). DRM inclinations are systematically shallow (Figure 8b), which is observed commonly in DRM redeposition experiments (e.g., Mitra & Tauxe, 2009). DRM intensities were normalized by k , ARM, and IRM (Figures 8d–8f) to remove the effects of magnetic mineral concentration. Samples from the inclusion-poor interval acquired a consistently stronger remanent magnetization than the inclusion-rich interval. In particular, IRM-normalized data have the most marked distinction between inclusion-rich and inclusion-poor samples (Figures 8d–8f).

5. Discussion

A paleomagnetic record from core MD01-2421 (Figure 4) and laboratory redeposition experiments for the same sediment (Figure 8) indicate that sediments containing significant magnetic mineral inclusions can record an ambient geomagnetic field. However, sedimentary magnetic inclusions are demonstrated here to record a weaker magnetization compared to samples that contain other forms of detrital magnetic

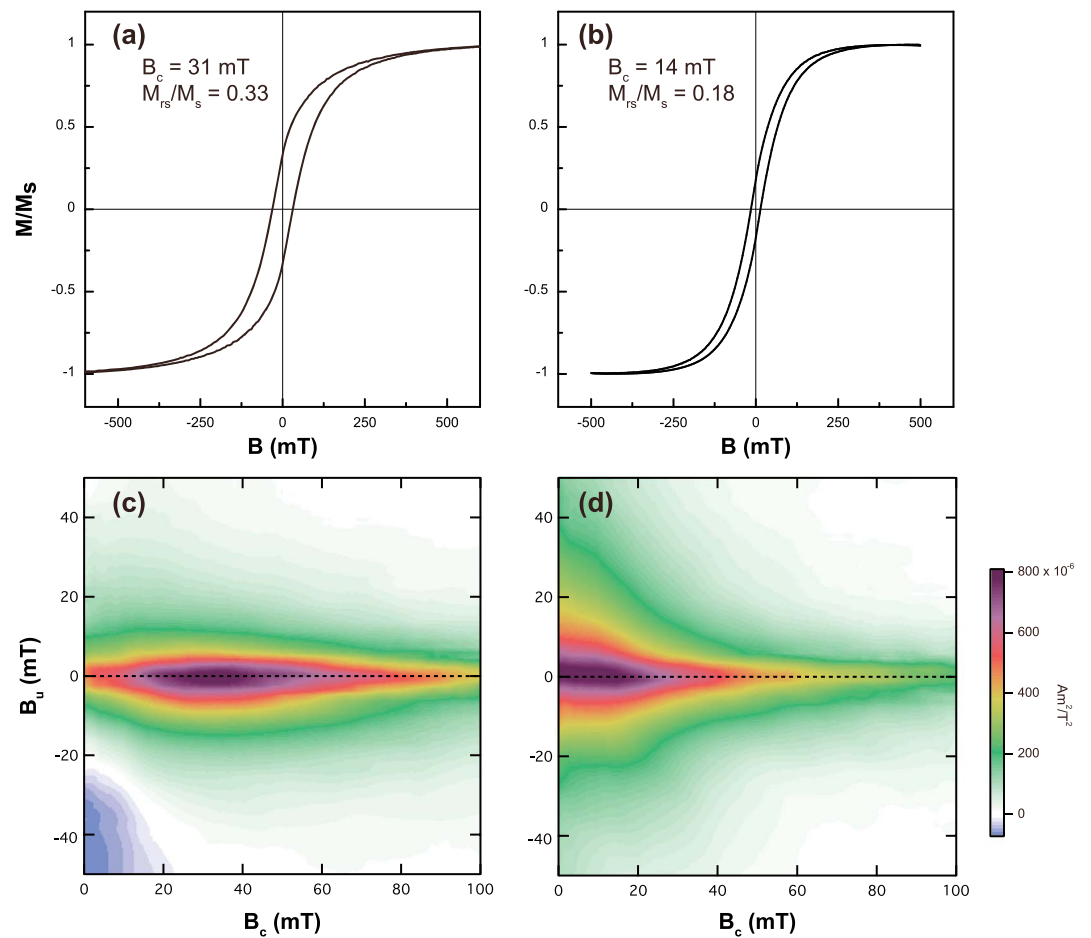


Figure 6. (a, b) Hysteresis loops and (c, d) first-order reversal curve diagrams for the two samples from (a, c) inclusion-rich (MD01-2421-10-100, 14.47 m, 42.91 ka) and (b, d) inclusion-poor (MD01-2421-16-100, 23.3 m, 71.43 ka) intervals, respectively, which were used for the redeposition experiments. Note that the loop for the inclusion-rich sample was measured to ± 1 T, but only a partial field range is shown. Hysteresis parameters (B_c and M_{rs}/M_s) are indicated. First-order reversal curve diagrams were processed with the variable smoothing FORC algorithm (VARIFORC) smoothing parameters (Egli, 2013): $\{sc0, sc1, sb0, sb1, \lambda_c, \lambda_b\} = \{6, 6, 4, 6, 0.1, 0.1\}$.

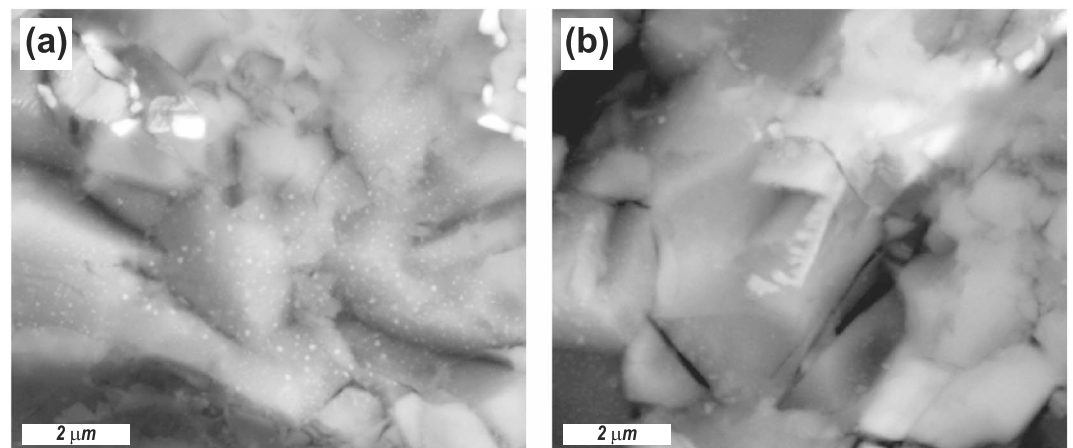


Figure 7. Scanning electron microscope images of magnetic extracts from an inclusion-rich sample (MD01-2421-10-100, 14.47 m, 42.91 ka). Observed morphologies of magnetic mineral inclusions include (a) nanoparticle clusters and (b) dendrites within silicates.

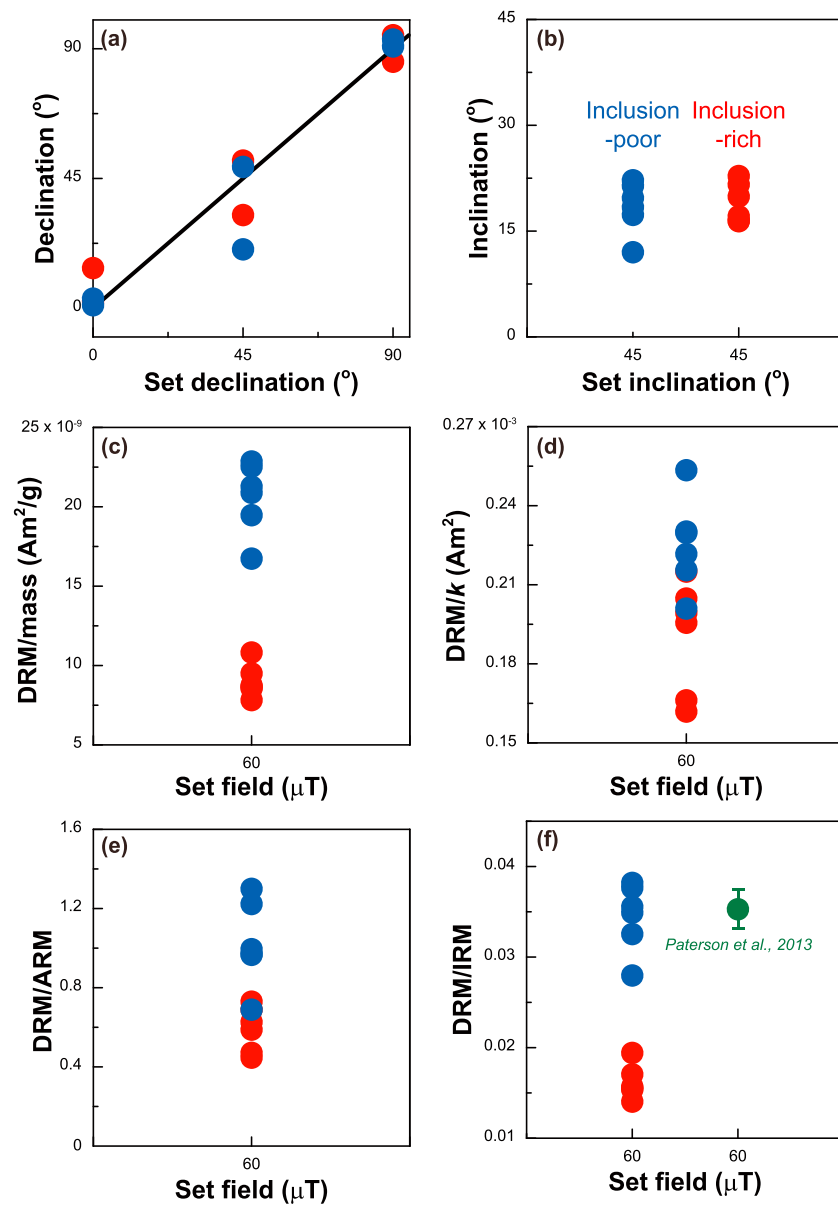


Figure 8. Results of laboratory redeposition experiments in a 60- μ T ambient field with set declination (0° , 45° , and 90°) and inclination (45°) for an inclusion-rich sediment sample (MD01-2421-10-100, 14.47 m, 42.91 ka, red) and an inclusion-poor sediment sample (MD01-2421-16-100, 23.3 m, 71.43 ka, blue) from core MD01-2421: subsamples from the magnetic inclusion-rich interval (red) and the inclusion-poor interval (blue). Stratigraphic positions of the selected samples are marked in Figure 2. The solid line is the expected declination trend. Acquisition of DRM (a) declination, (b) inclination, and intensity normalized by (c) mass, (d) susceptibility, (e) ARM, and (f) IRM compared with results from redeposition experiments for artificial sediments using magnetosomes (dark green: Paterson et al., 2013) and natural marine sediments (this study). DRM = detrital remanent magnetization; ARM = anhysteretic remanent magnetization; IRM = isothermal remanent magnetization.

minerals. Magnetic inclusions are embedded within larger nonmagnetic host silicates, which will have a weaker response to a geomagnetic torque than an equivalently small particle without a surrounding inclusion. The aligning geomagnetic torque competes with the hydrodynamic settling force during sediment deposition, and a weaker response to this aligning torque will produce a weaker net magnetization. Our data confirm this expectation and demonstrate the importance of magnetic inclusions for understanding the fidelity of sedimentary RPI records.

The small scatter of measured DRM declination data around the set declination value is likely caused by errors associated with orienting and measuring the redeposited cube samples (Figure 8a). The large inclination shallowing may be artificially enhanced due to the flat, hard bottom of the plastic cube surface and because the sediment forms a thin layer at the base of cube. Nevertheless, measured DRM inclination results cluster around values that are consistently shallower than the set value (Figure 8b).

The grain size of magnetic inclusions is smaller than unprotected detrital particles in the studied sediment core, so ARM and IRM are expected to be more sensitive to magnetic inclusions than k . This probably explains why the ARM and IRM normalized records are more similar to each other than to the k -normalized record (Figure 4). Results obtained in a 60- μ T applied field in our redeposition experiments and normalized by IRM are compared to results at the same applied field for artificial samples containing magnetosomes (Paterson et al., 2013; dark green, Figure 8f). IRM acquisition conditions and sediment concentrations have been ignored for our comparison (Figure 8f). It can be seen that our DRM/IRM results from inclusion-poor intervals are consistent with values from magnetosomes (Figure 8f), whereas inclusion-rich intervals are weaker than magnetosome results. These findings indicate different paleomagnetic recording efficiency for various constituent magnetic particle types, where magnetic inclusions within larger silicate particles have lower paleomagnetic recording efficiency. This confirms the results of Chen et al. (2017), which indicate that biogenic magnetite has a higher recording efficiency compared to detrital magnetic inclusions. More routine diagnosis of detailed relationships between detrital magnetic minerals and DRM recording is clearly needed to improve our understanding of sedimentary paleomagnetic signal recording.

Our results enable comparison of magnetic recording efficiency for sediment intervals that are dominated by magnetic inclusions and other forms of magnetic minerals and confirm that normalized remanence records for inclusion-rich intervals are affected by a recording bias toward weaker remanences compared to inclusion-poor intervals (Figure 4). Such inclusion-rich intervals can distort RPI by recording weaker remanences (Figure 4). As indicated by Roberts et al. (2012), such recording differences may not be constant throughout a sedimentary sequence because stratigraphically varying concentrations of different magnetic mineral types will produce variable DRM/ k , DRM/ARM, and DRM/IRM slopes (Figure 5). Thus, DRM records should be interpreted carefully, particularly considering the different magnetic mineral forms that occur in sediments and their contrasting magnetic recording efficiencies (e.g., Chen et al., 2017; Roberts et al., 2012). For example, biogenic magnetite has greater recording efficiency compared to detrital magnetite (Chen et al., 2017; Ouyang et al., 2014).

Recent studies demonstrate the widespread occurrence of different magnetic mineral types in sedimentary records. These different magnetic minerals can have different magnetic recording efficiencies (e.g., Chen et al., 2017; Ouyang et al., 2014). Further work is needed to recognize and characterize variable remanence acquisition efficiency associated with different magnetic mineral types, such as magnetic inclusions, and biogenic and detrital magnetic minerals. It is rare to find sediment sequences with a single and constant magnetic mineral assemblage, so suitable strategies for RPI normalization are needed for mixed magnetic mineral assemblages where the studied core fails the criteria for reliable RPI records (Tauxe, 1993).

6. Conclusions

Paleomagnetic data from marine sediment core MD01-2421 were analyzed by comparing the behavior of two types of distinct sediment intervals, where the magnetic signal in one is dominated by magnetic inclusions and the other is relatively poor in inclusions. Normalized remanence for the magnetic mineral inclusion-rich intervals generally records minima that are not observed in global RPI stacks. This is likely caused by the overall lower magnetization of silicate grains that contain magnetic inclusions. Such silicate hosts are not magnetic, and their larger size means that their response to a geomagnetic aligning torque will be counteracted more strongly by the hydrodynamic settling force. Our results indicate different paleomagnetic recording efficiencies for different detrital magnetic mineral types, where magnetic inclusions have lower recording efficiency. This conclusion is confirmed by redeposition experiments for natural sediments from magnetic inclusion-rich intervals and other intervals dominated by larger unprotected detrital magnetic grains. Contrasting DRM behavior is observed for these two sample types. In all cases, inclusion-poor intervals have stronger remanence than inclusion-rich intervals. Our results demonstrate that different detrital magnetic mineral types in sediments have different recording efficiency.

These observations have important implications for understanding the mechanisms of paleomagnetic recording and RPI normalization.

Acknowledgments

Data presented in this paper will be deposited in the MagIC database (<https://www2.earthref.org/MagIC>). This study was supported by the National Natural Science Foundation of China (Grants 41574060, 41574063, and 41722402) and the Australian Research Council (Grants DP120103952 and DP160100805). G. A. P. is supported by a NERC Independent Research Fellowship (NE/P017266/1). L. T. acknowledges support from NSF Grant EAR1547263. Our work on core MD01-2421 started with support from a grant from the Japan Society for the Promotion of Science to K. K. and A. P. R.

References

- Banerjee, S. K., King, J., & Marvin, J. (1981). A rapid method for magnetic granulometry with applications to environmental studies. *Geophysical Research Letters*, 8(4), 333–336. <https://doi.org/10.1029/GL008i004p00333>
- Blow, R. A., & Hamilton, N. (1978). Effect of compaction on the acquisition of a detrital remanent magnetization in fine-grained sediments. *Geophysical Journal of the Royal Astronomical Society*, 52(1), 13–23. <https://doi.org/10.1111/j.1365-246X.1978.tb04219.x>
- Canfield, D. E., Raiswell, R., & Bottrell, S. H. (1992). The reactivity of sedimentary iron minerals toward sulfide. *American Journal of Science*, 292(9), 659–683. <https://doi.org/10.2475/ajs.292.9.659>
- Carter-Stiglitz, B., Valet, J.-P., & LeGoff, M. (2006). Constraints on the acquisition of remanent magnetization in fine-grained sediments imposed by redeposition. *Earth and Planetary Science Letters*, 245(1–2), 427–437. <https://doi.org/10.1016/j.epsl.2006.03.002>
- Chang, L., Bolton, C. T., Dekkers, M. J., Hayashida, A., Heslop, D., Krijgsman, W., et al. (2016). Asian monsoon modulation of nonsteady state diagenesis in hemipelagic marine sediments offshore of Japan. *Geochemistry, Geophysics, Geosystems*, 17, 4383–4398. <https://doi.org/10.1002/2016GC006344>
- Chang, L., Roberts, A. P., Heslop, D., Hayashida, A., Li, J., Zhao, X., & Huang, Q. (2016). Widespread occurrence of silicate-hosted magnetic mineral inclusions in marine sediments and their contribution to paleomagnetic recording. *Journal of Geophysical Research: Solid Earth*, 121, 8415–8431. <https://doi.org/10.1002/2016jb013109>
- Channell, J. E. T., Xuan, C., & Hodel, D. A. (2009). Stacking paleointensity and oxygen isotope data for the last 1.5 Myr (PISO-1500). *Earth and Planetary Science Letters*, 283(1–4), 14–23. <https://doi.org/10.1016/j.epsl.2009.03.012>
- Chen, L., Heslop, D., Roberts, A. P., Chang, L., Zhao, X., McGregor, H. V., et al. (2017). Remanence acquisition efficiency in biogenic and detrital magnetite and recording of geomagnetic paleointensity. *Geochemistry, Geophysics, Geosystems*, 18, 1435–1450. <https://doi.org/10.1002/2016GC006753>
- Egli, R. (2013). VARIFORC: An optimized protocol for calculating non-regular first-order reversal curve (FORC) diagrams. *Global and Planetary Change*, 110, 302–320. <https://doi.org/10.1016/j.gloplacha.2013.08.003>
- Evans, M. E., McElhinny, M. W., & Gifford, A. C. (1968). Single domain magnetite and high coercivities in a gabbroic intrusion. *Earth and Planetary Science Letters*, 4(2), 142–146. [https://doi.org/10.1016/0012-821X\(68\)90008-3](https://doi.org/10.1016/0012-821X(68)90008-3)
- Feinberg, J. M., Harrison, R. J., Kasama, T., Dunin-Borkowski, R. E., Scott, G. R., & Renne, P. R. (2006). Effects of internal mineral structures on the magnetic remanence of silicate-hosted titanomagnetite inclusions: An electron holography study. *Journal of Geophysical Research*, 111(B12). <https://doi.org/10.1029/2006JB004498>
- Feinberg, J. M., Scott, G. R., Renne, P. R., & Wenk, H. (2005). Exsolved magnetite inclusions in silicates: Features determining their remanence behavior. *Geology*, 33(6), 513–516. <https://doi.org/10.1130/G21290.1>
- Guyodo, Y., & Valet, J. -P. (1999). Global changes in intensity of the Earth's magnetic field during the past 800 kyr. *Nature*, 399(6733), 249–252. <https://doi.org/10.1038/20420>
- Harrison, R. J., Dunin-Borkowski, R. E., & Putnis, A. (2002). Direct imaging of nanoscale magnetic interactions in minerals. *Proceedings of the National Academy of Sciences of the United States of America*, 99(26), 16,556–16,561. <https://doi.org/10.1073/pnas.262514499>
- Harrison, R. J., & Feinberg, J. M. (2008). FORCinel: An improved algorithm for calculating first-order reversal curve distributions using locally weighted regression smoothing. *Geochemistry, Geophysics, Geosystems*, 9, Q05016. <https://doi.org/10.1029/2008GC001987>
- Heslop, D. (2007). Are hydrodynamic shape effects important when modelling the formation of depositional remanent magnetization. *Geophysical Journal International*, 171(3), 1029–1035. <https://doi.org/10.1111/j.1365-246X.2007.03588.x>
- Heslop, D., Roberts, A. P., & Hawkins, R. (2014). A statistical simulation of magnetic particle alignment in sediments. *Geophysical Journal International*, 197(2), 828–837. <https://doi.org/10.1093/gji/ggu038>
- Heslop, D., Witt, A., Kleiner, T., & Fabian, K. (2006). The role of magnetostatic interactions in sediment suspensions. *Geophysical Journal International*, 165(3), 775–785. <https://doi.org/10.1111/j.1365-246X.2006.02951.x>
- Jackson, M., Banerjee, S. K., Marvin, J. A., Lu, R., & Gruber, W. (1991). Detrital remanence, inclination errors, and anhysteretic remanence anisotropy: Quantitative model and experimental results. *Geophysical Journal International*, 104(1), 95–103. <https://doi.org/10.1111/j.1365-246X.1991.tb02496.x>
- Katari, K., & Tauxe, L. (2000). Effects of pH and salinity on the intensity of magnetization in redeposited sediments. *Earth and Planetary Science Letters*, 181(4), 489–496. [https://doi.org/10.1016/S0012-821X\(00\)00226-0](https://doi.org/10.1016/S0012-821X(00)00226-0)
- King, R. F. (1955). The remanent magnetism of artificially deposited sediments. *Geophysical Supplements to the Monthly Notices of the Royal Astronomical Society*, 7(3), 115–134. <https://doi.org/10.1111/j.1365-246X.1955.tb06558.x>
- Levi, S., & Banerjee, S. K. (1990). On the origin of inclination shallowing in redeposited sediments. *Journal of Geophysical Research*, 95(B4), 4383–4389. <https://doi.org/10.1029/JB095iB04p04383>
- Lu, R., Banerjee, S. K., & Marvin, J. F. (1990). Effects of clay mineralogy and the electrical conductivity of water on the acquisition of depositional remanent magnetization in sediments. *Journal of Geophysical Research*, 95(B4), 4531–4538. <https://doi.org/10.1029/JB095iB04p04531>
- Mitra, R., & Tauxe, L. (2009). Full vector model for magnetization in sediments. *Earth and Planetary Science Letters*, 286(3–4), 535–545. <https://doi.org/10.1016/j.epsl.2009.07.019>
- Muxworthy, A. R., Evans, M. E., Scourfield, S. J., & King, J. G. (2013). Paleointensity results from the late-Archaeon Modipe Gabbro of Botswana. *Geochemistry, Geophysics, Geosystems*, 14, 2198–2205. <https://doi.org/10.1002/ggge.20142>
- Oba, T., Irino, T., Yamamoto, M., Murayama, M., Takamura, A., & Aoki, K. (2006). Paleooceanographic change off central Japan since the last 144,000 years based on high-resolution oxygen and carbon isotope records. *Global and Planetary Change*, 53(1–2), 5–20. <https://doi.org/10.1016/j.gloplacha.2006.05.002>
- Ouyang, T., Heslop, D., Roberts, A. P., Tian, C., Zhu, Z., Qiu, Y., & Peng, X. (2014). Variable remanence acquisition efficiency in sediments containing biogenic and detrital magnetites: Implications for relative paleointensity signal recording. *Geochemistry, Geophysics, Geosystems*, 15, 2780–2796. <https://doi.org/10.1002/2014GC005301>
- Paterson, G. A., Wang, Y., & Pan, Y. (2013). The fidelity of paleomagnetic records carried by magnetosome chains. *Earth and Planetary Science Letters*, 383, 82–91. <https://doi.org/10.1016/j.epsl.2013.09.031>
- Pike, C. R., Roberts, A. P., & Verosub, K. L. (1999). Characterizing interactions in fine magnetic particle systems using first order reversal curves. *Journal of Applied Physics*, 85(9), 6660–6667. <https://doi.org/10.1063/1.370176>

- Poultou, S. W., Krom, M. D., & Raiswell, R. (2004). A revised scheme for the reactivity of iron (oxyhydr)oxide minerals towards dissolved sulfide. *Geochimica et Cosmochimica Acta*, 68(18), 3703–3715. <https://doi.org/10.1016/j.gca.2004.03.012>
- Quidelleur, X., Valet, J. -P., LeGoff, M., & Boudoire, X. (1995). Field dependence on magnetization of laboratory-redeposited deep-sea sediments: First results. *Earth and Planetary Science Letters*, 133(3–4), 311–325. [https://doi.org/10.1016/0012-821X\(95\)00088-T](https://doi.org/10.1016/0012-821X(95)00088-T)
- Renne, P. R., Scott, G. R., Glen, J. M. G., & Feinberg, J. M. (2002). Oriented inclusions of magnetite in clinopyroxene: Source of stable remanent magnetization in gabbros of the Messum Complex, Namibia. *Geochemistry, Geophysics, Geosystems*, 3(12), 1079. <https://doi.org/10.1029/2002GC000319>
- Roberts, A. P. (2015). Magnetic mineral diagenesis. *Earth-Science Reviews*, 151, 1–47. <https://doi.org/10.1016/j.earscirev.2015.09.010>
- Roberts, A. P., Almeida, T. P., Church, N. S., Harrison, R. J., Heslop, D., Li, Y., & Zhao, X. (2017). Resolving the origin of pseudo-single domain magnetic behavior. *Journal of Geophysical Research: Solid Earth*, 122, 9534–9558. <https://doi.org/10.1002/2017jb014860>
- Roberts, A. P., Chang, L., Heslop, D., Florindo, F., & Larrasoana, J. C. (2012). Searching for single domain magnetite in the “pseudo-single-domain” sedimentary haystack: Implications of biogenic magnetite preservation for sediment magnetism and relative paleointensity determinations. *Journal of Geophysical Research*, 117(B8). <https://doi.org/10.1029/2012JB009412>
- Roberts, A. P., Florindo, F., Chang, L., Heslop, D., Jovane, L., & Larrasoana, J. C. (2013). Magnetic properties of pelagic marine carbonates. *Earth-Science Reviews*, 127, 111–139. <https://doi.org/10.1016/j.earscirev.2013.09.009>
- Roberts, A. P., Pike, C. R., & Verosub, K. L. (2000). First-order reversal curve diagrams: A new tool for characterizing the magnetic properties of natural samples. *Journal of Geophysical Research*, 105(B12), 28,461–28,475. <https://doi.org/10.1029/2000JB900326>
- Selkin, P. A., Gee, J. S., Tauxe, L., Meurer, W. P., & Newell, A. J. (2000). The effect of remanence anisotropy on paleointensity estimates: A case study from the Archean Stillwater Complex. *Earth and Planetary Science Letters*, 183(3–4), 403–416. [https://doi.org/10.1016/S0012-821X\(00\)00292-2](https://doi.org/10.1016/S0012-821X(00)00292-2)
- Shcherbakov, V. P., & Sycheva, N. (2010). On the mechanism of formation of depositional remanent magnetization. *Geochemistry, Geophysics, Geosystems*, 11, Q02Z13. <https://doi.org/10.1029/2009GC002830>
- Shcherbakov, V. P., & Sycheva, N. K. (2008). Flocculation mechanism of the acquisition of remanent magnetization by sedimentary rocks. *Izvestiya-Physics of The Solid Earth*, 44(10), 804–815. <https://doi.org/10.1134/S106935130810008X>
- Spassov, S., & Valet, J.-P. (2012). Detrital magnetizations from redeposition experiments of different natural sediments. *Earth and Planetary Science Letters*, 351–352, 147–157. <https://doi.org/10.1016/j.epsl.2012.07.016>
- Tarduno, J. A., & Cottrell, R. D. (2005). Dipole strength and variation of the time-averaged reversing and nonreversing geodynamo based on Thellier analyses of single plagioclase crystals. *Journal of Geophysical Research*, 110(B11), B11101. <https://doi.org/10.1029/2005jb003970>
- Tarduno, J. A., Cottrell, R. D., & Smirnov, A. V. (2006). The paleomagnetism of single silicate crystals: Recording geomagnetic field strength during mixed polarity intervals, superchrons, and inner core growth. *Reviews of Geophysics*, 44, RG1002. <https://doi.org/10.1029/2005RG000189>
- Tarduno, J. A., Cottrell, R. D., Watkeys, M. K., Hofmann, A., Doubrovine, P. V., Mamajek, E. E., & Usui, Y. (2010). Geodynamo, solar wind, and magnetopause 3.4 to 3.45 billion years ago. *Science*, 327(5970), 1238–1240. <https://doi.org/10.1126/science.1183445>
- Tauxe, L. (1993). Sedimentary records of relative paleointensity of the geomagnetic field: Theory and practice. *Reviews of Geophysics*, 31(3), 319–354. <https://doi.org/10.1029/93RG01771>
- Tauxe, L., Steindorf, J. L., & Harris, A. (2006). Depositional remanent magnetization: Toward an improved theoretical and experimental foundation. *Earth and Planetary Science Letters*, 244(3–4), 515–529. <https://doi.org/10.1016/j.epsl.2006.02.003>
- Ueshima, T., Yamamoto, M., Irino, T., Oba, T., Minagawa, M., Narita, H., & Murayama, M. (2006). Long term Aleutian Low dynamics and obliquity-controlled oceanic primary production in the mid-latitude western North Pacific (Core MD01-2421) during the last 145,000 years. *Global and Planetary Change*, 53(1–2), 21–28. <https://doi.org/10.1016/j.gloplacha.2006.01.017>
- Usui, Y., Shibuya, T., Sawaki, Y., & Komiya, T. (2015). Rock magnetism of tiny exsolved magnetite in plagioclase from a Paleoproterozoic granitoid in the Pilbara craton. *Geochemistry, Geophysics, Geosystems*, 16, 112–125. <https://doi.org/10.1002/2014GC005508>
- Valet, J.-P., Meynadier, L., & Guyodo, Y. (2005). Geomagnetic dipole strength and reversal rate over the past two million years. *Nature*, 435(7043), 802–805. <https://doi.org/10.1038/nature03674>
- Valet, J.-P., Tiant, C., & Carlot, J. (2017). Detrital magnetization of laboratory-redeposited sediments. *Geophysical Journal International*, 210(1), 34–41. <https://doi.org/10.1093/gji/ggx139>
- Van Vreumingen, M. J. (1993a). The magnetization intensity of some artificial suspensions while flocculating in a magnetic field. *Geophysical Journal International*, 114(3), 601–606. <https://doi.org/10.1111/j.1365-246X.1993.tb06990.x>
- Van Vreumingen, M. J. (1993b). The influence of salinity and flocculation upon the acquisition of remanent magnetization in some artificial sediments. *Geophysical Journal International*, 114(3), 607–614. <https://doi.org/10.1111/j.1365-246X.1993.tb06991.x>
- Zhao, X., Egli, R., Gilder, S. A., & Muller, S. (2016). Microbially assisted recording of the Earth's magnetic field in sediment. *Nature Communications*, 7, 10673. <https://doi.org/10.1038/ncomms10673>
- Ziegler, L. B., Constable, C. G., Johnson, C. L., & Tauxe, L. (2011). PADMM2M: A penalized maximum likelihood model of the 0–2 Ma palaeomagnetic axial dipole moment. *Geophysical Journal International*, 184(3), 1069–1089. <https://doi.org/10.1111/j.1365-246X.2010.04905.x>